DOI: https://doi.org/10.14311/TPFM.2025.001

AXISYMMETRIC JET UNDER ACTIVE CONTROL BY COAXIAL SYNTHETIC JET

Z. Antošová[1], B. Arhens[2], J. Pech[1]

[1] Department Thermodynamics, Institute of Thermomechanics of the CAS, Dolejškova 1402/5, Prague 8, 18200, Czech Republic

[2] Nantes Université Graduate School of Engineering (Polytech Nantes), Rue Christian Pauc CS 50609, 44306 Nantes, France

Abstract

Axisymmetric continuous air jet issuing from a long straight pipe nozzle was actively controlled using coaxially placed annular synthetic jet. The Reynolds numbers of the main and control jets were kept constant, 5000 and 750, respectively. The topic was studied experimentally using PIV technique and numerically using commercial software FLUENT. It was shown that active control induces large-scale stream-wise velocity fluctuation, increases axial velocity and prolongs the potential core of the main jet.

Keywords: active control, axisymmetric jet, synthetic jet

1 Introduction

Fluid flow control can be a powerful tool in many fluid mechanics and convective heat transfer tasks. While the passive control requires no additional energy and is usually low-cost solution, the active control, i.e. application of some type of additional energy into the main (controlled) jet flow offers wider range of operational regimes. One of the active control possibilities is an application of periodic forcing at one or more frequencies. This approach aims at amplification of the (coherent) structures naturally present in the jet flow.

Crow and Champagne [1] introduced the term "preferred mode", as the natural frequency of the jet, in other words, the Strouhal number, St_0, at which the jet is the most sensitive to an external excitation. Following the work by Crow and Champagne, the topic of preferred mode (or also column mode) has been studied since then and it has been revealed that there is not one value of preferred mode but rather a range of Strouhal numbers, in which the preferred mode lies, see e.g. Thomas [2], St_0 = (0.25-0.85).

The present work is a follow-up to a previous research focused on control of round jet with synthetic jet (SJ) as the control jet in the region of rather low Reynolds numbers (Re = 1000-5000), see Antošová and Trávníček [3], where especially the effect of the control on jet's intermittency factor and intensity of turbulence was studied using hot-wire anemometry. The current study is aimed at an entire flowfield of both control and controlled jets using mainly PIV measurement. In addition, the possibilities of flow simulation of this particular geometry are also explored using simple 2D model.

2 Experimental setup and methods

Figure 1(a) shows the scheme of the investigated geometry. The main jet issues from a long straight pipe with inner diameter D = 10.05 mm and length of 75D. The pipe is oriented vertically, and the flow direction is from top to bottom. The working fluid was air. The inlet of the pipe was equipped with a honeycomb to suppress the rotational component of the velocity. The flow rate was measured using rotameter installed upstream of the test section.

The SJ actuator consists of a sealed cavity equipped with an electrodynamically actuating diaphragm of diameter D_D = 53 mm, which was built from MONACOR SP-7/4S loudspeaker. The outer and inner diameters of the annular nozzle are D_o = 15.05 mm and D_i = 11.95 mm, respectively. The actuator is fed by a sinusoidal current from the sweep/function generator (RIGOL DG4062) with the audio amplifier (PIONEER A-209R). The frequency and power input were kept constant, f = 246 Hz and P = 2.23 W, respectively. A more detailed description of the experimental setup can be found in [3].

The PIV experiment was made in the 500 mm x 500 mm x 600 mm transparent (PMMA) box. An aerosol is used for seeding (DEHS-DANTEC DYNAMICS liquid) with droplet sizes between 1 and 3 μm. The PIV system comprises a double-pulsed Nd:YAG laser (Litron, NANO 145–15 PIV, 532 nm)

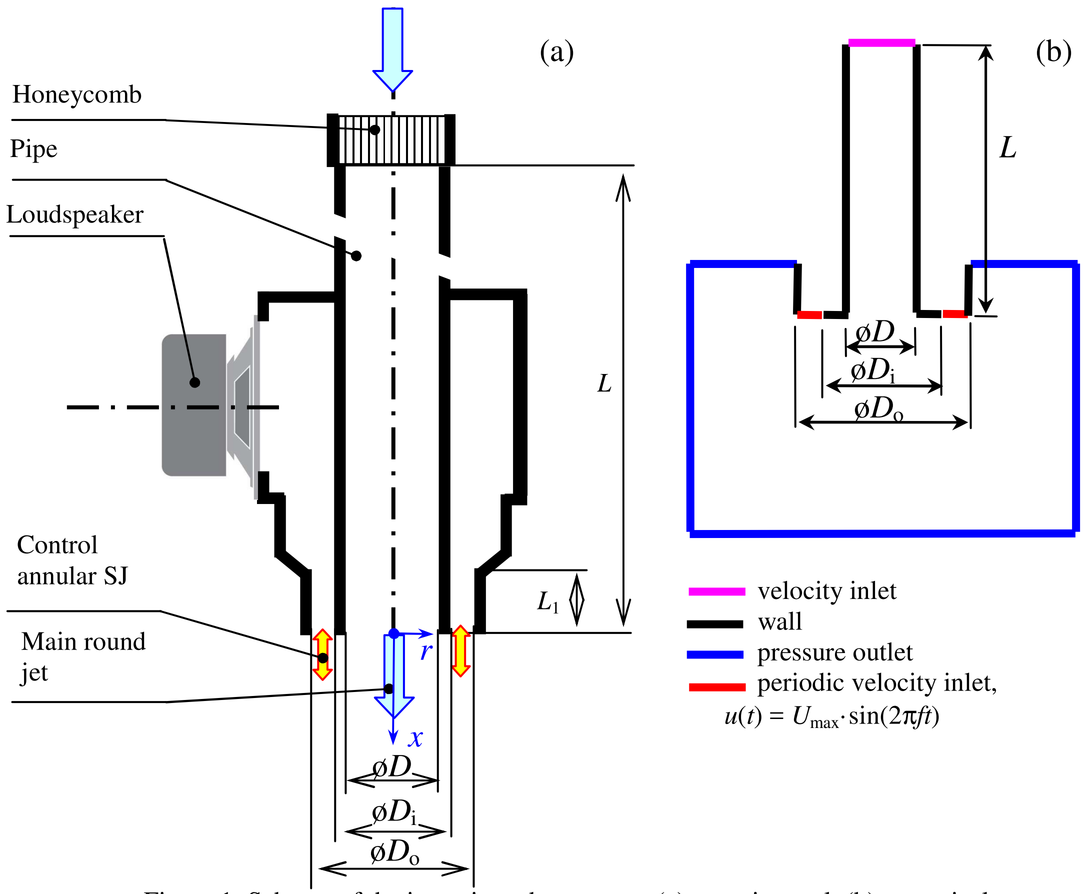

Figure 1: Scheme of the investigated geometry, (a) experimental, (b) numerical.

with cylindrical optics. The time delay between the pulses varied between 10 and 50 μs. The images were recorded by a high resolution digital camera (HiSense Neo, 2560 x 2160 pixels, 16 bit) equipped with a Tokina 100 mm F2.8 Macro D lens. For time-mean flow field evaluation, the sampling frequency was set at 15 Hz. The PIV system was synchronised with function generator using its second channel. This setup allows capturing the periodic process of SJ actuation at chosen phase of the working cycle, i.e. the phase-locked mode. For the PIV system operation and subsequent data post-processing, the Dynamic Studio software was utilized. The pictures were post-processed using adaptive cross-correlation technique (with IA between 8 and 32 px and 50% overlap) and filtered using moving average validation. In every run (both in time-mean and phase-locked mode) 100 pictures were taken, so the resulting pictures represent the average flowfield (time-mean or phase-locked time-mean).

PIV technique was also used for flow visualization. In this case, the density of seeding particles was kept higher than for PIV velocity measurement.

Some auxiliary measurement was also done using hot-wire anemometry method in constant temperature mode (for more detailed description of the method and setup see [3]) and by the Pitot probe.

3 Computational setup and methods

For the numerical simulation, the commercial software FLUENT 2023R1 and 2024R1 was utilised. For this preliminary numerical study, a simplified 2D simulation was proposed. Mesh, consisting of about 44000 cells included refinement toward the tube walls and in vicinity of the synthetic jet. The scheme of the computational geometry and boundary conditions is presented in Fig. 1(b). In this simplified model the cavity of the synthetic jet actuator was not modelled. The simulation of the main jet without control was done in steady setup, while transient incompressible solver was used for jet control simulation. The time-step was chosen d$t \approx 0.0005$ accordingly to requested 8 steps per period. Default parameters were left in k-omega-SST model of turbulence. Boundary conditions: main jet - velocity inlet, uniform velocity profile, control jet - time-dependent, uniform velocity profile. The velocity magnitude was prescribed wave given by: $u(t) = U_{max} \cdot \sin(2\pi f\, t)$, where t is the time, $U_{max} = 12$ m/s and $f = 246$ Hz. The tube walls were subject for no-slip boundary condition, outer parts of the domain were set to the pressure-outlet.

4 Parameters

The flow rate of the main jet was kept constant, Q = 36.8 l/min. The resulting exit mean velocity is thus U_m = 7.8 m/s. The Reynolds number of the main jet is given by $Re = U_m D/\nu$, where ν is the kinematic viscosity. The Reynolds number of the SJ is given as $Re_{SJ} = U_0 D_{SJ}/\nu$, where $D_{SJ} = (D_o - D_i)$ is a hydraulic diameter of the annular nozzle and U_0 is extrusion orifice velocity averaged over the entire cycle: $U_0 = \frac{1}{T}\int_0^{T_E} u_0(r=0,t)\,dt$. The characteristic SJ velocity was evaluated from previous hot-wire anemometry measurement (see [3]), U_0 = 3.83 m/s (Re_{SJ} = 754). The ratio of the control and main jet velocity was $c_u = U_0/U_m$ = 0.49. The Strouhal number of the control process is defined as $St = fD/U_m$. The parameters of the SJ (P and f) were chosen to set the ratio c_u at approximately 0.5 and the St close to the expected preferred mode of the main jet, i.e. St = 0.3, see [1].

5 Results

5.1 Main jet

Figure 2(a) shows visualization of the main jet instantaneous flow field (without control). In agreement with Reynolds number, the jet is turbulent in character, with visible vortical structures and mixing in the shear layer. The gradual increase in the jet width caused by intensive entrainment can be observed as well. The measured time-mean velocity field of the main jet in Fig. 2(b) confirms the above described qualitative observation - the jet is reasonably symmetrical with rather flat (turbulent) velocity profile close to the pipe exit and widens gradually further downstream. In Fig 2(c) the distribution of the velocity magnitude obtained from the numerical simulation reveals expected structure of the pipe jet flow - potential core of the jet in the nearfield and its gradual vanishing due to entrainment of the surrounding fluid.

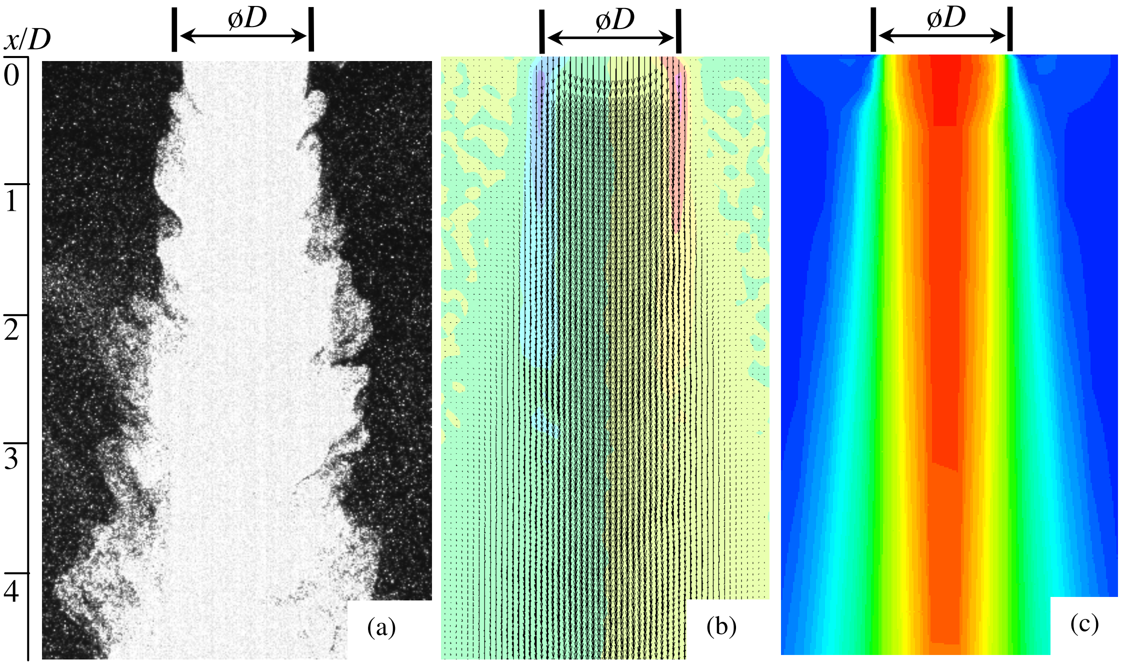

Figure 2: Main jet (without control), (a) visualization, (b) experiment (colored with vorticity contours, for scale, see Fig. 6) , (c) simulation.

The evolution of axial velocity magnitude (i.e. r = 0) from experiment and simulation is compared in Fig. 3(a). The typical regions can be identified. In the nearfield there is the potential core visible as the region of constant velocity. With the end of the core, the axial velocity starts to decay. The end of the potential core was evaluated from PIV at x/D = 2.6 (where U/U_m = 0.95). The simulation sets the end of the core a bit downstream at x/D = 3.8. The velocity decay slope for the experimental data agrees well with theoretical decay in the far field of the axisymmetric turbulent jet, $U/U_m \approx (x/D)^{-1}$, see [4]. On the other

other hand, the calculated decay is significantly slower, with a slope approximately $U/U_{max} \approx (x/D)^{-0.5}$, which corresponds rather to a decay of turbulent plane jet. These results are in accord with current numerical (2D) model, which is not able to catch the intensive mixing process (and thus faster jet spreading and axial velocity decrease) caused by 3D jet interaction with its surroundings.

Figure 3(b) presents exit velocity profile of the jet (without control), the velocity is normalized by maximum (axial) velocity, U_{p_max}. The empirical dimensionless profile based on power-law with an exponent of 1/7 is plotted as well. In agreement with *Re*, the profile is rather flat and the numerical profile agrees well with experimental profile and also with the empirical one.

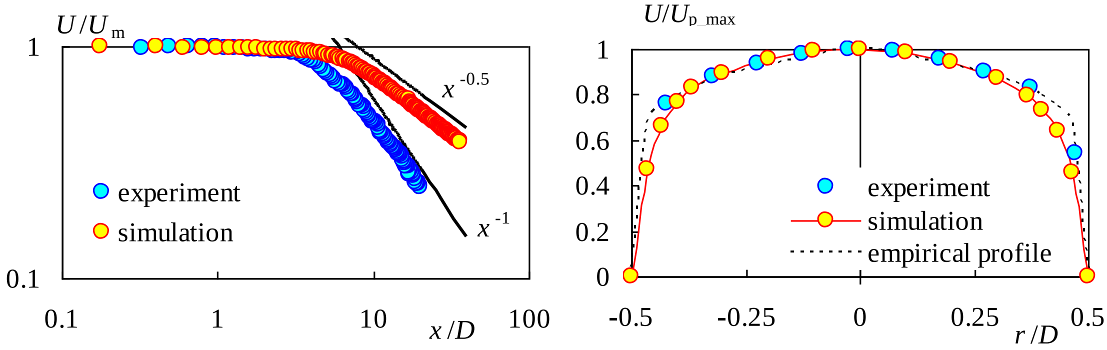

Figure 3: Main jet (without control), (a) axial velocity decay, (b) exit velocity profile.

5.2 Control jet

Experimentally obtained (phase-locked) vector fields of the SJ at maximum extrusion and suction are shown in Fig. 4. A pair of coaxial vortex rings is formed at the output of SJ actuator. This phenomenon is visible in 2D PIV plane as two vortex pairs. During the period, the vortex rings propagate further downstream, their diameters are getting smaller and the inner ring gradually disappears completely with the end of the jet's recirculation area.

Unsteady character of the jet can be seen in Fig. 5 where the streamwise component of the axial velocity during one period is plotted. Similarly to annular continuous jets, three jet regions can be distinguished: initial (recirculation) area (region of the negative axial velocity in the very nearfield), intermediate merging zone, where the point of reattachment can be found, and fully merged region (farfield). Giving the periodic nature of the SJ, the positions of the end of the recirculation area (x_c) and the point of reattachment (x_r) vary with phase of the period. The large-scale fluctuation of the velocity gradually fades away and disappears completely around x/D = 3.5 (see also Fig. 4).

5.1 Main jet under active control

Velocity vector fields of actively controlled jet obtained from a phase-locked PIV measurement are presented in Fig. 6(a) and (b). Again, the pair of pictures shows the flowfield at maximum extrusion and suction of the control SJ. Similarly to the solo-standing control jet, the inner vortex ring of the SJ disappears rapidly, while the outer one travels downstream. Surprisingly, the ring does not merge easily with the main jet, but rather slides along the outer main jet's mixing layer and gradually slows down and lose its coherence (i.e. similarly to behaviour of the SJ in Fig. 4).

Although the control jet does not merge with the main jet in the nearfield, the SJ affects the main jet considerably. The streamwise component of the axial velocity of the jet is plotted in Fig. 7(a). The periodical character of the control jet triggers the formation of the large-scale velocity fluctuation in the main jet. While the periodic character of the solo-standing SJ can be distinguished up to approximately x/D = 3.5, in the case of the controlled main jet, this character persists up to approximately x/D = 7. The control jet causes the periodic contraction at passage of the vortex ring and consequent stretching of the main jet resulting in the regions of higher and lower streamwise velocity. However, this periodic behaviour of the jet has no significant impact on the cross-stream velocity component, for which no organized pattern was identified. The control affects also the time-mean flowfield of the jet, the end of the potential core is moved slightly downstream from x/D = 2.6 to x/D = 3.2 and the axial velocity increases, in the region from x/D = 5 to 20 the average increase is 14%. The comparison of the experimental and numerical time-mean results is plotted in Fig. 7(b). The axial velocity from simulation is lower in the very nearfield, however, it does not decrease as fast as the experimental curve. This phenomenon is similar to the previous observation for the main jet without control in Fig. 3(a), i.e. the 2D model is not able to catch the intensive mixing processes, which are obviously 3D in character. Unlike the experimental results, the simulation predicts local axial velocity increases around x/D = 1, indicating that the contraction/stretching effect of the control on the main jet is more accented in numerical results. However, the deeper study to explain the discrepancy is needed.

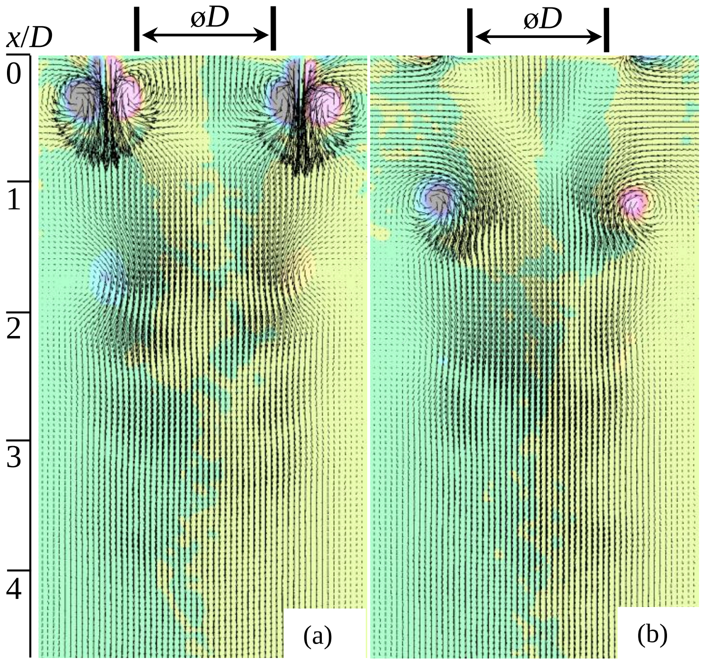

Figure 4: Control (synthetic) jet, (a) maximum extrusion, 45°, (b) maximum suction, 225° (scale - Fig. 6).

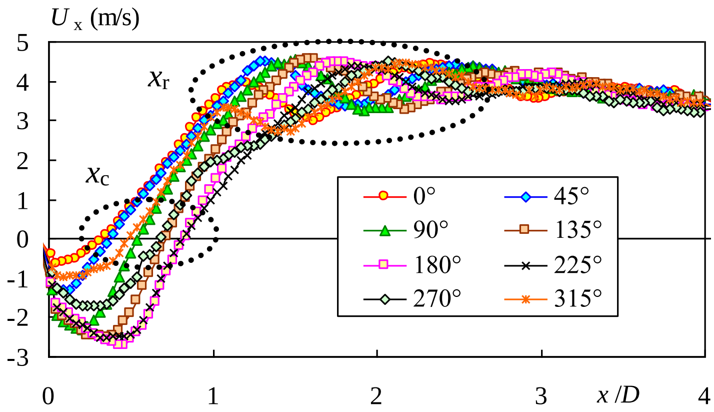

Figure 5: Streamwise component of axial velocity of control jet during 1 period.

6 Conclusions

The low-turbulent round jet under active control was studied, both experimentally and numerically. The results have shown that the round jet can be successfully controlled using annular synthetic jet. Using the control, the large-scale fluctuation of the main jet axial streamwise velocity was obtained. The time-mean axial velocity increased and the potential core was prolonged. The comparison of the experimental data with the simple 2D numerical model has shown that the numerical model gives results which are in reasonable agreement with the experimental ones, however, to obtain the data which reflect the reality more closer, the more sophisticated 3D model would be needed for this, rather complex, geometry.

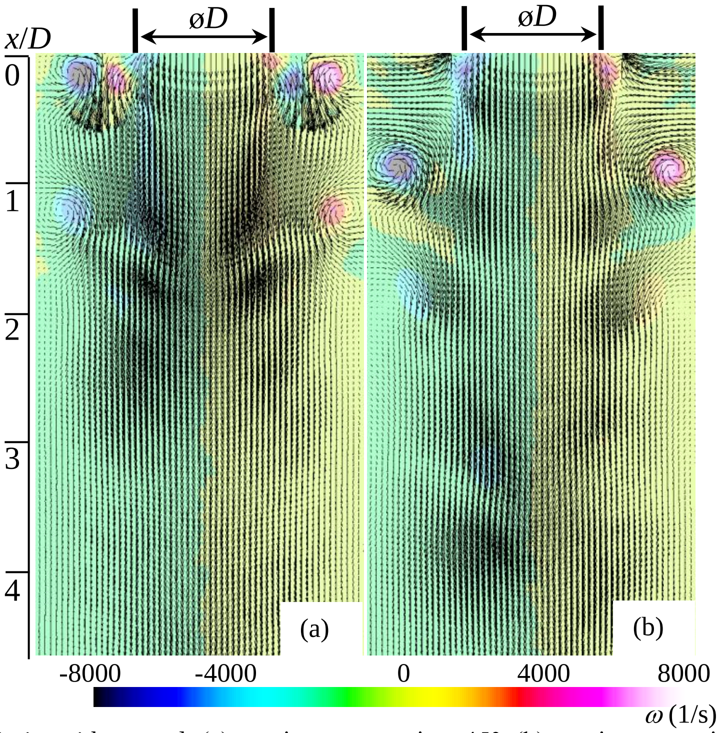

Figure 6: Main jet with control, (a) maximum extrusion, 45°, (b) maximum suspension, 225°.

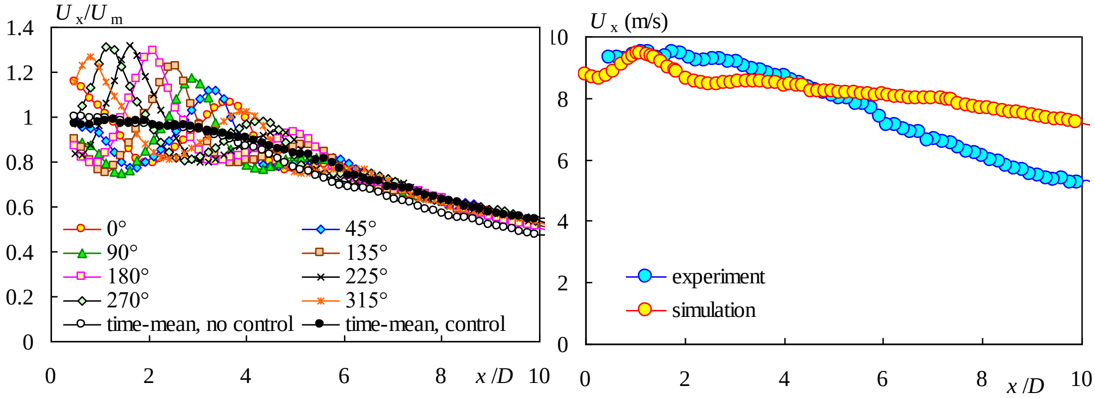

Figure 7: Streamwise component of axial velocity of the main jet with control, (a) experiment, (b) time-mean experiment and simulation comparison.

Acknowledgment

We gratefully acknowledge the support of the Czech-Taiwanese cooperation based on the Agreement on Scientific Cooperation between the Czech Academy of Sciences (NSTC-24–03) and the National Science and Technology Council (NSTC-113-2927-I-002-514), the Internal project of the Institute of Thermomechanics (902 167) and the institutional support of the Institute of Thermomechanics (RVO: 61388998)

References

[1] Crow, S.C. & Champagne, F.H.: Orderly structure in jet turbulence. *J. Fluid Mech.*, 48(1971), pp. 547–591.

[2] Thomas, F.O.: Structure of mixing layers and jets. *Appl. Mech. Rev.*, 44(1991), pp. 119–153.

[3] Antošová, Z. & Trávníček, Z.: Control of a round jet intermittency and transition to turbulence by means of an annular synthetic jet, *Actuators*, 10:185(2021).

[4] Blevins, R.D.: Applied Fluid Dynamics Handbook; Krieger Publishing: Malabar, FL, USA, 2003.